Trefoil Factor 3 Overexpression in Prostatic Carcinoma: Prognostic Importance Using Tissue Microarrays

Dennis A. Faith,[1] William B. Isaacs,[1,3] James D. Morgan,[2] Helen L. Fedor,[2] Jessica L. Hicks,[2] Leslie A. Mangold,[1] Patrick C. Walsh,[1] Alan W. Partin,[1] Elizabeth A. Platz,[4] Jun Luo,[1]** and Angelo M. De Marzo[1,2,3]*

[1]*Brady Urological Institute, The Johns Hopkins University, School of Medicine, Baltimore, Maryland*
[2]*Department of Pathology, The Johns Hopkins University, School of Medicine, Baltimore, Maryland*
[3]*The Sidney Kimmel Comprehensive Cancer Center, The Johns Hopkins University, School of Medicine, Baltimore, Maryland*
[4]*Department of Epidemiology, Johns Hopkins University, Bloomberg School of Public Health, Baltimore, Maryland*

BACKGROUND. Human intestinal trefoil factor 3 (TFF3) is a member of a family of polypeptides encoded by a cluster of genes on chromosome 21. Through gene expression profiling studies TFF3 mRNA has been found to be overexpressed in prostate cancer.
METHODS. We used immunochemistry on tissue microarrays and software tools, collectively referred to as TMAJ, for online assessment of staining to analyze samples from 294 primary tumors and 61 metastatic lesions.
RESULTS. Applying a cutoff of 20% of cells staining as positive, the frequency of staining was 18.8% in normal (51 of 272) and 47.0% in primary tumors (126 of 268), $P < 0.0001$, Wilcoxon rank sum). Expression of TFF3 in metastatic prostate cancer was similar to that in primary tumors. TFF3 expression was not associated with time to biochemical recurrence, development of distant metastasis, or death due to prostate cancer. Scoring data derived from visual estimation of expression correlated highly with semi-automated image analysis using the Automated Cellular Imaging System (ACIS™) from Chromavision, Inc.
CONCLUSIONS. These studies validate that TFF3 is overexpressed at the protein level in a subset of primary and metastatic prostate cancers, show the first use of the TMAJ database, and demonstrate the ability to semi-automatically scan and score immunohistochemically stained tissue microarray slides.

KEY WORDS: **prostate cancer; tissue microarrays; trefoil factor**

INTRODUCTION

Human intestinal trefoil factor (TFF3, gene symbol *hITF*) is a member of a family of polypeptides characterized by containing at least one copy of the trefoil motif, a 3-leaved structure formed by three conserved disulfides within a 40-amino acid segment [1,2]. Trefoil peptides are expressed mainly in gastrointestinal and

Grant sponsor: NIH/NCI (Public Health Services); Grant number: R01CA084997; Grant sponsor: Goodwin family (philanthropic support); Grant sponsor: The Commonwealth Foundation for Cancer Research; Grant sponsor: NIH/NCI Specialized Program in Research Excellence (SPORE) in Prostate Cancer; Grant number: P50CA58236; Grant sponsor: The Prostate Cancer Foundation; Grant sponsor: Susan and Donald Sturm (Philanthropic Support).

*Correspondence to: Angelo M. De Marzo, MD, PhD, Department of Pathology, The Johns Hopkins University, CRB 153, 1650 Orleans Street, Baltimore, MD 21231-1000. E-mail: ademarz@jhmi.edu

**Correspondence to: Jun Luo, PhD, Marburg 411, Brady Urological Institute, The Johns Hopkins University School of Medicine, 600 N. Wolfe Street, Baltimore, MD 21287.
E-mail: jluo1@jhmi.edu
Received 7 January 2004; Accepted 26 January 2004
DOI 10.1002/pros.20095

other selected epithelial tissues and are packaged along with mucins and secreted [3–5]. TFF3 was first identified in the rat intestine [6] and is constitutively expressed in the goblet cells of the small and large intestine [1,3,7]. TFF3 was later characterized for its role in reconstitution of an epithelial barrier after mucosal injury in the jejunum [8]. During the mucosal restitution process, TFF3 is required to maintain the integrity of the mucosal barrier to protect the epithelial layer against environmental insult, as well as, for promotion of wound repair by enhancing epithelial dispersion at sites of injury [9–11]. These characteristics have led to association of aberrant TFF3 peptide expression with a number of chronic inflammatory diseases including Crohn's disease, ulcerative colitis, and cholecystitis [12,13]. In addition, TFF3 has also been shown to function as an epithelial anti-apoptotic factor, and neural signaling peptide [4,14,15]. TFF3 expression has also been documented in other tissues including the uterus [16], breast [17], hypothalamus/pituitary [15,18], salivary glands [19,20], conjunctiva [21,22], and respiratory tract [22,23].

Alterations in TFF3 expression have been observed in cancer cells, with overexpression reported in breast carcinoma [17,24], gastric carcinoma [25], mucinous pancreatic tumors [26], and both primary and metastatic colo-rectal carcinoma [27]. Although the role of TFF3 in neoplasms remains unclear, its expression correlates with poor prognosis in gastric carcinoma [28]. While the related trefoil protein, TFF1, has been reported to be over-expressed in prostate cancer tissues [29,30], the present study, along with an accompanying paper by Garaway et al. [31] represent the first demonstration of TFF3 overexpression in prostate cancer.

In the original studies using mRNA expression profiling of Luo et al. [32], and in two other datasets as well [33–35], TFF3 mRNA was found to be consistently up-regulated in the majority of prostate cancer specimens as compared to benign prostate tissue. The present study was performed to validate TFF3 overexpression at the protein level. In addition, using tissue microarrays containing a large number of specimens from primary prostate cancer and novel software tools for online TMA image scoring (TMAJ [36,37]), we investigated the relation of TFF3 expression to pathological variables and its potential prognostic value. For prognostic studies we used a group of patients, all of whom developed biochemical recurrence (consistently elevated serum PSA) after radical prostatectomy, to correlate TFF3 expression levels with time to biochemical recurrence, development of clinical metastases (positive bone scan), and death due to prostate cancer. Finally, as an initial demonstration of semi-automated image analysis of conventional bright field microscopy images of TMA spots, the visual estimation of immunostaining of TMA spots was compared with results obtained using an Automated Cellular Imaging System (ACIS^{TM} I) [38–41] from ChromaVision Medical Systems.

MATERIALS AND METHODS

Tissue Microarray Patient Selection and Construction

A total of 294 radical prostatectomy samples were selected from the Surgical Pathology files at The Johns Hopkins Department of Pathology with Institutional Review Board approval. Two groups were chosen. Group I contained 133 patients selected arbitrarily from approximately 400 sequential cases performed between January 2000 and August 2001. Since the follow-up time was short for these patients, we only examined TFF3 expression in relation to preoperative serum prostate specific antigen (PSA) levels, and the pathological variables of Gleason grade and stage at radical prostatectomy. Group II contained 161 cases selected arbitrarily from a series of 304 cases obtained between 1982 and 1996 [42] with complete follow up information. Median follow-up in this group was 8 years. All patients in Group II developed biochemical recurrence, and a subset of these patients also developed clinically evident distant metastases ($n = 48$) or died from metastatic prostate cancer ($n = 33$). An additional array was constructed that consisted of metastatic prostate cancer tissue obtained by searching the archives of Surgical Pathology at Johns Hopkins Hospital for distant metastases. The metastatic tissue microarray contained 61 cases, including 51 lymph node metastases, three bone metastases and seven soft tissue metastases. None of these patients were treated with hormonal therapy before surgery.

Tissue microarrays were prepared as previously described [43,44]. Areas representing a portion of the largest, and/or highest grade carcinoma present, as well as areas of normal appearing prostatic epithelium from each case were circled on H&E stained glass slides. For each sample, a standard section was first immunostained with $p27^{Kip1}$ as a measure of adequate fixation [45]. In the vast majority of carcinoma cases, tumor areas were selected only if surrounded by normal appearing prostate epithelium, where strong $p27^{Kip1}$ staining of nuclei of luminal secretory cells was evident. Areas of normal were selected only if they contained moderate or strong nuclear $p27^{Kip1}$ staining in the majority of luminal epithelial cells. In all cases, tissue fixation was performed with neutral buffered formalin. For the Group II cases, fixation was generally performed by immersing whole prostates in formalin overnight prior to sectioning the prostate. For the Group I cases, the fixation was generally performed by

formalin injection as described [45,46], or by placing relatively small portions of tissue in fixative to facilitate rapid fixation [47]. For each patient's specimen, four cores of tumor and four cores of normal tissue were placed into TMAs.

TMAJ as a Tissue Microarray Analysis Platform

A set of software tools and underlying relational database was developed to accommodate patient information storage, specimen data, paraffin block data, tissue microarray data, tissue microarray construction, and online image assessment and data export [36,37] Additional information can be found at http://www.tmaj.pathology.jhmi.edu/. The structure of the relational database, evolved from the original Prostate Specialized Program of Research Excellence (SPORE) model [48].

Visual image assessment tools were developed using the Sun Microsystems Java platform and are deployed over the internet using the Java Network Launching Protocol (JNLP) via Java™ Web start. Java Web Start retains many of the benefits of a traditional browser markup language's user interface, such as using a network URL as a launching point and automatically updating client applications. The Java Web start programs, while being launch-able from a web browser, run as stand-alone applications that are web browser independent. Images were scanned using the Bacus Laboratories Image Scanning System (BLISS) and each TMA spot was exported as a composite image as previously reported [48–50]. The images were then copied to a secure server, where links to the images were created in the Sybase database using the TMAJ-Import program. Images were then viewed over the internet on a personal computer using the TMAJ-Image application. The TMAJ-Image application supports the simultaneous side-by-side display of TMA spots stained with different stains on adjacent sections. This feature was used to compare 5 μm TMA sections stained against TFF3 with an adjacent 5 μm TMA that was doubly labeled against both alpha-methylacyl-CoA racemase (AMACR) and p63 [50]. P63 is a marker of basal cell nuclei in the prostate, which are characteristically absent in prostatic adenocarcinoma, and AMACR is a cytoplasmic marker that is elevated in expression in the majority of prostate cancers. All cases scored as carcinoma had an absence of basal cells in the specific glands evaluated, and the majority of the carcinoma cells were simultaneously positive for AMACR. A third slide, stained with standard hematoxylin and eosin was also available for simultaneous viewing. Diagnosis and stain quality assessments were assigned directly to the database. Another feature of the TMAJ-Image application supports random presentation of array spot images. This feature was used to minimize scoring bias based on array sample location. The scoring data were then linked to the pathology data and exported in text format, using the data export function of the TMAJ-Image application, for statistical analysis using Stata 8.0 for Microsoft Windows.

Semi-Automated Image Acquisition and Analysis Using the ACIS

In addition to visual analysis, TFF3 expression levels in a subset of arrays were evaluated using the Chromavision ACIS I system (Chromavision Medical Systems, Inc., San Juan Capistrano, CA). The ACIS I system (version 2.30) consists of a computer controlled bright-field microscope coupled to a CCD camera capable of simultaneously detecting levels of hue (color), saturation (density), and luminosity (darkness). Using the ACIS software, threshold values for each parameter are optimized to permit color intensity based spectral resolution via a proprietary color-space transformation. The learn-by-example tool in the ACIS software package was used to train the system to separately recognize brown pixels (immunoreactivity) and blue pixels (counterstain). Threshold variables were adjusted until masked brown pixels visually correlated with immuno-positive epithelial cytoplasm and masked blue pixels correlated with areas of pure counter-stain in stromal tissue.

Since different TMA spots contained variable percentages of stromal tissue, we employed a normalization scheme involving comparing positive TFF3 staining area to the area of epithelial tissue as delineated by cytokeratin 8 (CK8) on adjacent TMA slides. A total of six TMA slides, three each for TFF3 and CK8 staining, were scanned using the standard TMA template parameters for the ACIS system plus the pre-assembled array-specific topology file. Post-scan analysis began with optimization of software color recognition thresholds. Threshold values were established for scoring the brown staining detecting TFF3 and CK8 immunopositivity. For each array, threshold values were adjusted such that any appreciable immunopositivity was detected as brown pixels (brown area), while interspersed and adjacent counterstain was detected separately as blue pixels (blue area). The blue area was thresholded to detect stromal cytoplasm only and used simply to compare similarity of adjacent cores—if counterstain deviated significantly, cores were excluded from analysis. For each pair of slides a value for TFF3 brown area and an adjacent CK8 brown area were generated and exported to an excel spreadsheet. After export, a normalized value was calculated as the fraction of epithelial area staining positively in each TMA core by dividing TFF3

brown area by CK8 brown area. To assess the efficacy of comparing adjacent sections for cytoplasmic immunostains, a pair of TMA slides separated by 20 μm were stained with CK8, then optimized and processed as above. The data generated for brown area between these two immunostains showed a tight correlation ($r = 0.99$), indicating that comparison of adjacent sections is a viable and reproducible method to quantify area of staining from tissue microarray spots.

Western Blotting

A total of 50 frozen sections 10 μm in thickness were cut and placed into conical tubes. The sections were solubilized in Laemmli sample buffer minus β-mercaptoethanol and Bromophenol Blue. Protein was quantified using the BCA reagent method (Pierce Biotechnology, Inc., Rockford, IL). Forty micrograms of solubilized protein was subjected to SDS–polyacrylamide (8–16% gradient) gel electrophoresis. Samples were transferred to nitrocellulose via semi-dry transfer using the discontinuous CAPS buffer system (Bio-Rad Laboratories, Hercules, CA). The blot was subsequently probed with the anti-TFF3 mouse monoclonal antibody (Calbiochem, clone 15C6/IgG1, San Diego, CA) at a 1:100 dilution. Detection was conducted using the enhanced chemiluminescence ECL kit (Amersham Biosciences, Piscataway, NJ).

Immunohistochemical Staining

Staining for TFF3 was carried out using the Envision + kit (Dako Corp., Carpentaria, CA). Deparaffinized slides were dehydrated and then placed in citrate buffer (pH 6.0) and steamed for 20 min. Endogenous peroxidase activity was quenched by incubation with Dako peroxidase block for 5 min at room temperature. Slides were then washed and incubated with primary antibody (1:50 dilution of antiserum) for 1 hr at 4°C. Secondary anti-mouse antibody-coated polymer peroxidase complex was applied for 30 min at room temperature. Substrate/chromogen (3,3′-diaminobenzidine [DAB]) was applied and incubated for 5 min at room temperature. Slides were then counterstained with Mayer's hematoxylin.

For double labeling of AMACR and p63, slides were prepared as above and incubated with the anti-AMACR antibody (1:16,000 dilution of antiserum) overnight at 4°C. The anti-p63 mouse monoclonal antibody cocktail (1:100 dilution; Lab Vision Corp., Fremont, CA) was added after the anti-racemase antibody incubation, and incubated for 45 additional minutes at room temperature. The secondary anti-rabbit and anti-mouse HRP conjugates were mixed and added together, and the reaction was developed as above.

Slides stained with CK8 for automated cellular analysis were prepared as above and incubated with the anti-CK8 antibody (1:800 dilution; InnoGenex, San Ramon, CA) at room temperature for 45 min. The secondary anti-mouse HRP conjugate and chromogen were applied as above.

Matching TMA slides were prepared as above and incubated with the anti-chromagranin A (1:3,200 dilution; Chemicon International, Inc., Temecula, CA) antibodies for 45 min. Secondary incubation, chromogen, and counterstain were performed as described above.

Visual Estimation of Immunohistochemical Analysis

Due to the variable nature of TFF3 staining in terms of number of positive cells and intensity of staining, a three-variable scoring strategy was developed. These three primary criteria were used to evaluate the score of all samples without knowledge of clinical or pathological features. For each TMA spot a pathologic diagnosis was assigned based on H&E morphology and AMACR/p63 staining. Second, the percentage of cells in the given TMA spot with the assigned diagnosis staining above background was estimated and recorded as the percentage of positive cells for TFF3 staining. Next, the percentage of cells with the pathologic diagnosis that exhibited very intense staining was estimated (see Figs. 1, 2). This value was then recorded as the percentage of strongly positive cells.

Statistical Analysis

TFF scoring data was examined in relation to radical prostatectomy Gleason score, pathological stage, surgical margin involvement, and pre-operative serum PSA. Clinical follow up data in Group II included time to biochemical recurrence, development of distant metastasis, and death due to prostate cancer. Comparative analysis was conducted using the Wilcoxon rank-sum (non-parametric) and the Kruskal–Wallis test (non-parametric) when multiple populations were compared.

RESULTS

Western Blot and Immunohistochemistry Analysis of Control Tissue

TFF3 protein has been previously shown to be expressed in colon tissue while being absent in normal gastric epithelium [28]. A Western blot was performed using fresh protein extracts of colon and normal gastric tissues obtained as flash frozen tissue from surgical specimens. Figure 1A shows a specific band at approximately 8 kDa, consistent with the expected size, that was present in colon tissue and absent in normal

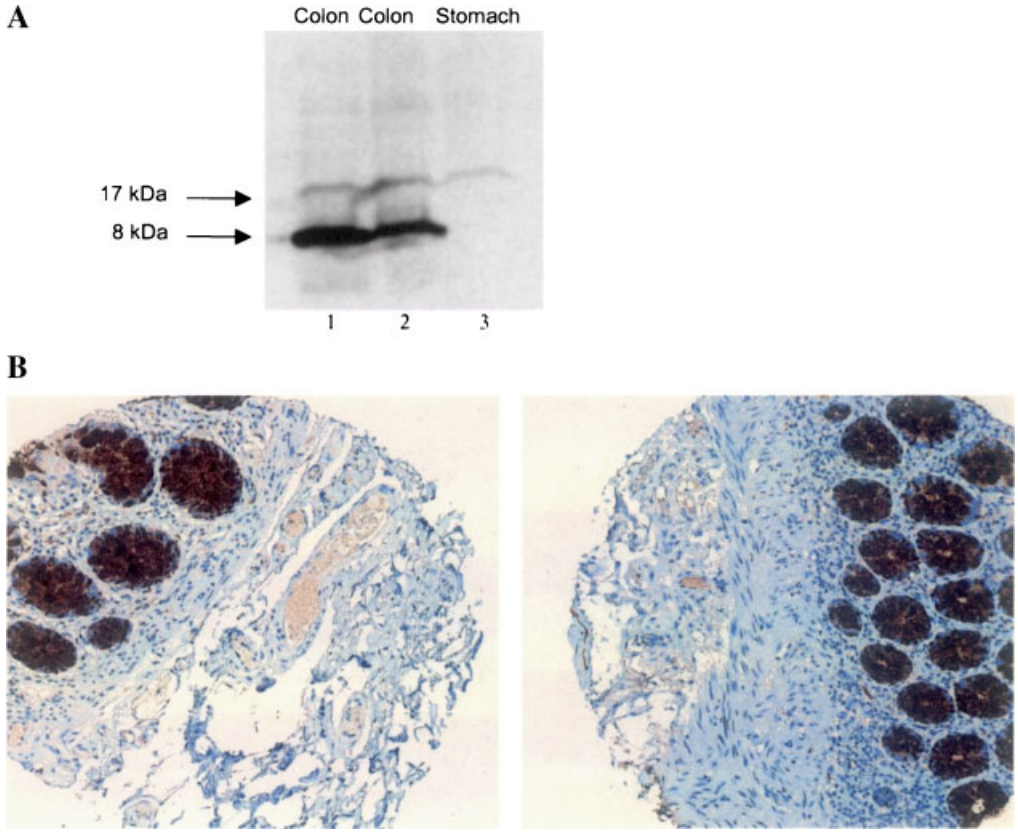

Fig. 1. Western blot and immunohistochemisty against trefoil factor 3 (TFF3) in control tissues. **A**: Western blot against TFF3 in normal colon and stomach tissue. Normal colon from two different patients (**lanes 1** and **2**). Normal gastric tissue (**lane 3**). **B**: Immunohistochemical staining against TFF3 expression in two different normal colon samples. This is an example of strong intensity staining restricted to epithelial cells. Original magnification ×100. [Color figure can be viewed in the online issue, which is avaliable at www.interscience.wiley.com.]

gastric epithelium. A second much less intense 17 kDa band was present in both tissue types and was considered non-specific. Immunohistochemistry using this antibody showed strong intensity staining in normal colonic epithelium (Fig. 1B) and negative staining in gastric epithelium (not shown).

IHC Analysis of Radical Prostatectomy Specimens UsingTMAs

TMAs were constructed (n = 7) to contain clinically localized prostate cancer and matched normal appearing epithelium from 294 patients who underwent radical prostatectomy. Table I contains a summary of clinical and pathological data for these patients. Figure 2 shows a screenshot of the TMAJ Image application showing some of the features of this software program, such as the ability to display thumbnail and full size images and the ability to view adjacent TMA spots on the same computer screen. For the entire study, 2,972 TMA spots were imaged. Two thousand four hundred fifty nine (82.7%) produced usable data and 513 (17.3%) were not useful. The 513 unused images contained prostate stroma only (162), or uninterpretable images (74 diagnoses not clear, 57 images out of focus, 170 no tissue in image, and 50 had scant tissue). Of the usable images, 485 (19.7%) represented internal control tissues, 155 (6.3%) contained metastatic sites and 1,819 (74.0%) tumor-normal comparison spots. Of the prostate images, 836 were carcinoma, 854 were normal epithelium, 95 were simple atrophy and 34 were high-grade prostatic intraepithelial neoplasia (PIN). The distribution of the frequencies of tumor grade of the TMA spots from primary tumors scored was Gleason 3: 533 (63.8%), Gleason 4: 225 (26.9%), Gleason 5: 57 (6.8%), intraductal carcinoma: 10 (1.2%), colloid (mucinous) carcinoma: 9 (1.1%), and 1 each of pseudohyperplastic and atrophic carcinoma (0.12%).

Examples of staining of TFF3 in prostate tissues are shown in Figures 2 and 3. In all cases staining was restricted to the epithelial compartment with no stromal cell staining in either tumor or normal tissues. In normal epithelium, two patterns of staining were found. The first pattern was cytoplasmic staining occurring in a variable number of lumenal epithelial cells (Figs. 2, 3). The intensity of this staining was generally weak/moderate (Fig. 3A, B), but was occasionally strong (Fig. 3C). The second pattern was that of

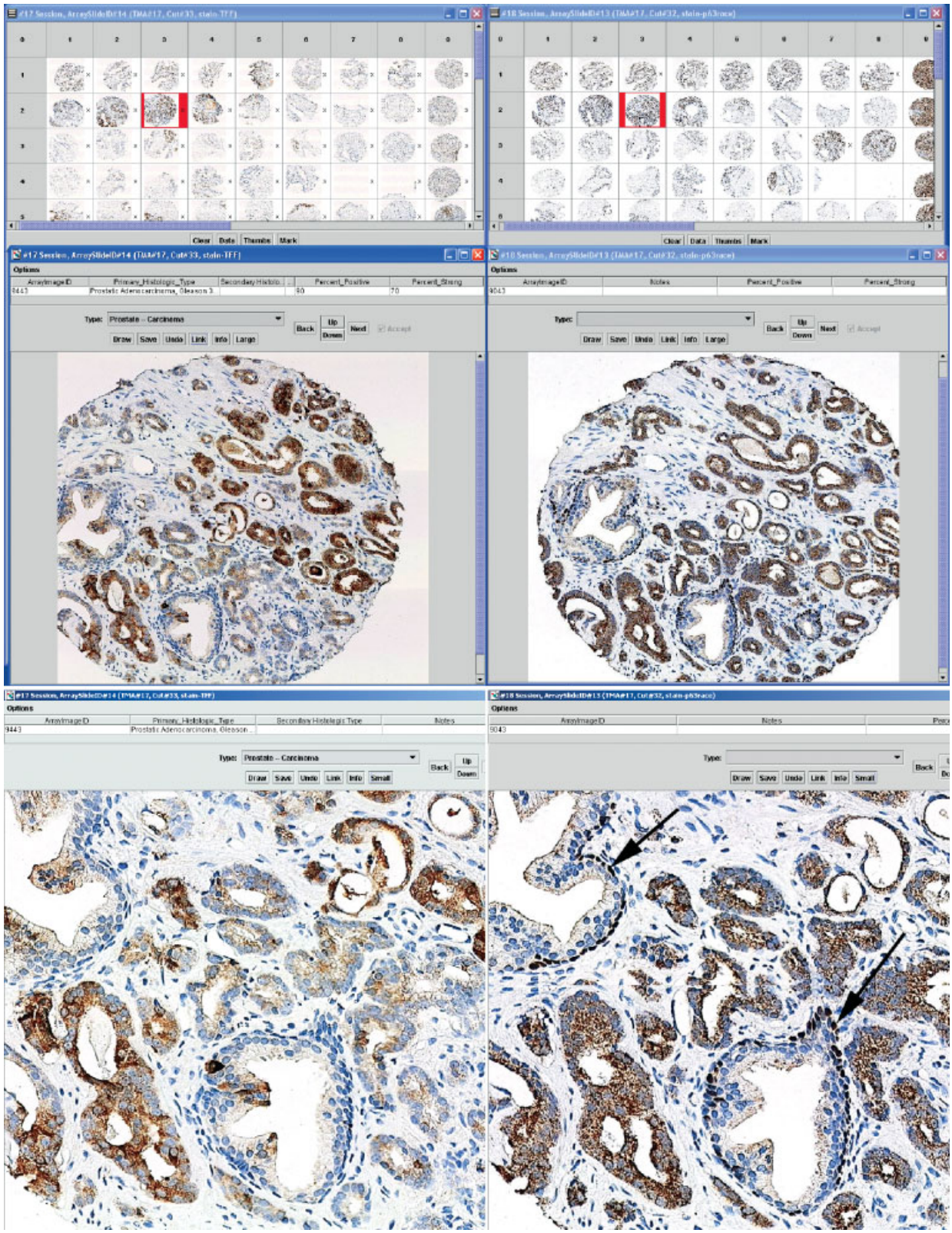

Fig. 2. Screenshots of TMAJ Image application. **Top two panels** show thumbnail views of part of adjacent 5 μm TMA sections stained with TFF3 (**left**) and P63/Racemase (**right**). Arrays stained with each antibody were from adjacent sections. **Middle panels** show corresponding larger images. Images are diagnosed using pull down menus and scores are typed into the correct fields. Tumor cells show both strong and weak staining for TFF3, and diffuse strong staining for racemase. **Bottom panels** show that images can be zoomed to high power. Arrows indicate p63 positive benign glands, which are negative for racemase. Images, such as this, with both tumor and normal tissue were scored visually only for tumor tissue. Original magnification in **lower panels**, ×200.

TABLE I. Clinico-Pathological Characteristics of Radical Prostatectomy (RRP) Patients With Tissues Available on Evaluated TMA Spots

Number of patients	294
Patient age at RRP	
Mean ± SD	59.0 ± 6.35
Median	59
Range	42–74
Preoperative PSA (ng/ml)	
Mean ± SD	9.94 ± 8.07
Median	7.9
Range	0.1–55.2
Pathological data	
Stage	n
pT2	102 (37%)
pT3a	97 (36%)
pT3b	36 (13%)
N1	38 (14%)
Total	273 (100%)
Gleason score	
5–6	100 (35%)
7	118 (42%)
8–10	65 (23%)
Total	283 (100%)

Stage and grade data are from radical prostatectomy specimens. Totals for stage and Gleason score do not add up to 294 due to missing TMA spots or uninterpretable TMA Images or unavailability of complete clinical data.

intense staining in scattered dendriform cells that were generally present in the basal compartment (Fig. 3F). This latter pattern of staining was suggestive of neuroendocrine cells (see description of neuoendocrine cell staining below).

Tumor tissue showed markedly increased staining as compared to matched normal tissue ($P < 0.0001$, Wilcoxon Rank-Sum) (Fig. 3C–E). The average number of usable TMA spots analyzed was 3.1 for both tumor and normal. A mean score for each diagnostic category (tumor or normal) was calculated for percent positive and percent strong for each patient [50]. These mean of these means or scores were used for all statistical analyses. Figure 4 shows the distribution of the mean scores for percentage of epithelial cell staining for normal and tumor using the radical prostatectomy specimens. The mean percent positive staining for normal (n = 272 different patient samples) was 11.2 (SD 17.0) and that for tumor (n = 268 different patient samples) was 35.8 (SD 37.7). The mean percent strong staining for normal was 3.1 (SD 8.3) and for tumor was 21.0 (SD 32). Using a cutoff of 20% of epithelial cells staining above background to consider a specimen positive, the frequency of normal specimens staining positive was 51/272 (18.8%), whereas the frequency of positive staining in tumor tissues was 126/268 (47.0%) (Wilcoxon Rank Sum, $P < 0.0001$). Using a 20% cut-off value for strong positive staining, the frequency of cases staining strongly in normal was 13/272 (4.8%), while that for tumor tissue was 84/272 (31.3%) (Wilcoxon Rank Sum, $P < 0.0001$). A summary of these data appear in Table II.

Relation of TFF3 Staining to Pathological Variables at Radical Prostatectomy and to Clinical Outcome

When combining both Group I and Group II (n = 294, Table III), there was an inverse correlation between TFF3 expression (mean percent positive cells) and overall pathological stage, as well as presence of extraprostatic extension (capsular penetration), seminal vesicle invasion, and pelvic lymph node metastasis. However, when the two groups were analyzed separately, the inverse correlation between TFF3 levels and pathological stage was only apparent in Group II (data not shown). In Group II patients there was no relation between levels of TFF3 expression and time to biochemical recurrence, presence of distant metastasis, or death due to prostate cancer (Tables III, IV).

Comparison of Visual Estimation of Percentage of Cells Staining With Automated Image Analysis Using the ACIS I

A subset of three TMA slides that were scanned with the BLISS workstation and scored visually were rescanned using the ACIS TMA application. This application allows the user to define a grid that is overlaid onto an image of the TMA. For each identified TMA spot, quantitative data regarding area and intensity of brown staining was generated. For this study, we only used the brown area data and not intensity data. Data for each TMA spot was then exported as a Microsoft Excel spreadsheet and linked to the previously collected image diagnosis data. A total of 717 TMA spots were usable for analysis. To ensure an accurate assessment of the epithelial area staining positively in each TMA core with assigned diagnosis, TMA spots known to contain both tumor and normal tissues (n = 82) were eliminated, and percent positive scores were calculated by dividing TFF3 brown area by total area of epithelium defined by CK8 staining. Automated scoring data of the remaining TMA spots (n = 635) by the ACIS I correlated highly with the visual estimation of percent positive staining ($r = 0.84$, $P = <0.0001$) (Fig. 5). TFF3 showed clear overexpression in tumor samples when compared to normal tissues using the data generated from the ACIS I (Wilcoxon Rank Sum, $P < 0.0001$).

Intense Staining of Neuroendocrine-Like Cells

The dendriform cells with intense TFF3 staining were recognized in 335 TMA spots representing 156 of the 294 cases. These cells were present in normal

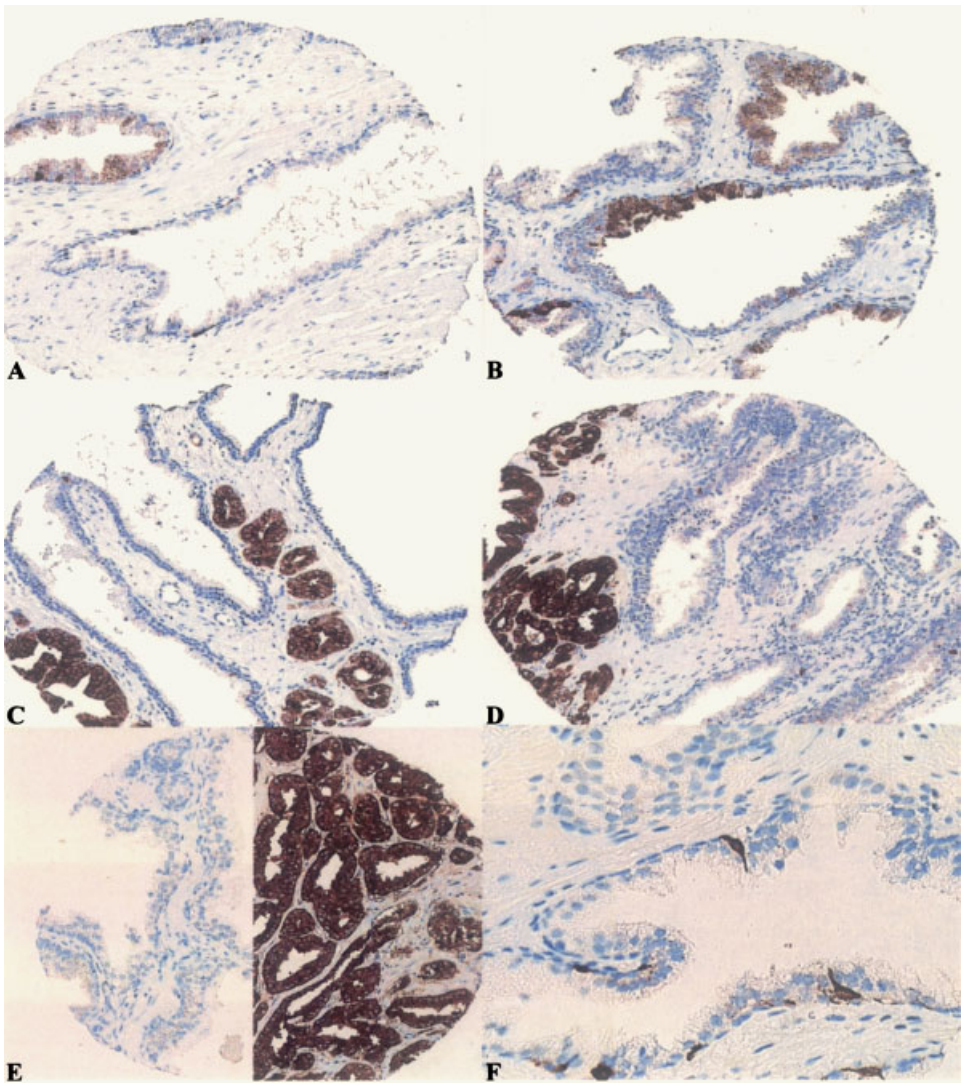

Fig. 3. TFF3 expression in normal prostate epithelium and prostate cancer. **A**, **B**: Heterogeneous low intensity staining expression in normal epithelium. **C**, **D**: Strong TFF3 staining restricted to tumor cells, with normal appearing epithelium staining negatively. **E**: Another normal (**left**), tumor (**right**) pair. **F**: Strong staining in dendriform cells in normal epithelium. Original magnification ×200 (A–E), and ×400 (F). [Color figure can be viewed in the online issue, which is avaliable at www.interscience.wiley.com.]

appearing epithelium in 150 cases, but were present in the cancer in only six cases. To provide further evidence that these cells represent neuroendocrine cells, an adjacent section of one of the TMAs was stained with chromogranin A. Although there were somewhat more cells staining with chromagranin A, the pattern of staining for dendriform cells was similar, supporting the hypothesis that the dendriform cells staining intensely positively for TFF3 are of neuroendocrine origin (data not shown). Further support comes from the positive staining for TFF3 in pancreatic islet cells (see below).

IHC Analysis of Prostate Cancer Metastases

TFF staining was analyzed in prostate cancer metastases from a total of 61 patients (3 bone, 51 lymph nodes, and 7 soft tissue). The mean percent positive staining in metastatic tissue was 35.9 (SD 39.0), whereas the mean percent strong was 19.3 (SD 30.7) (Table II). Thus, the staining of metastatic prostate cancer lesions was similar to that of primary carcinomas.

TFF3 Protein Expression in Other Tissues

Several normal human tissues that were included on the TMAs as controls showed staining for TFF3. In addition to goblet cells in the colon and ileum, the vast majority of epithelial cells from thyroid showed strong cytoplasmic staining for TFF3, as did minor laryngeal mucin-secreting salivary glands. The endocrine pancreas (islets) was weakly positive in most cells. Thymus, spleen, tonsil (both epithelium and lymphoid

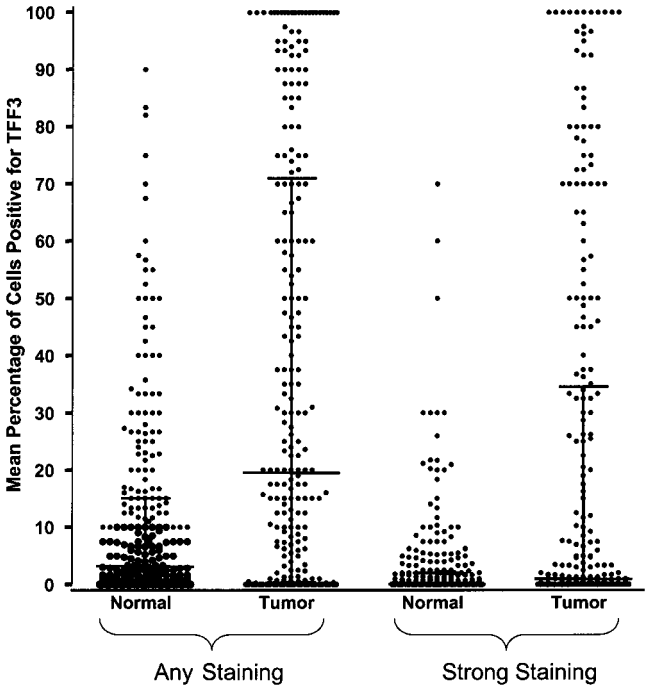

Fig. 4. Distribution of values for visual estimation of percent of cells staining positive for TFF3 protein (tumor vs. normal comparisons, $P < 0.0001$, Kruskal–Wallis). The individual data points represent the mean percentage of positive cells of TMA spots from each patient from each tissue type (tumor and normal). The horizontal bars represent the median and inter-quartile range. On the left side the data points represent the mean for spots with any TFF staining regardless of intensity, and on the right side the points represent only those cases with strong intensity staining.

tissue), skin, skeletal muscle, smooth muscle (from multiple organs), kidney, bladder, esophagus, brain (gray and white matter and cerebellar cortex), seminal vesicle, and testis were all negative (data not shown).

DISCUSSION

In this study, we demonstrate by immunohistochemistry that TFF3 is overexpressed in a subset of primary and metastatic prostate cancer specimens. This work, therefore, validates another candidate gene discovered to be overexpressed at the mRNA level using RNA expression profiling of frozen clinical samples of prostate tissue. This work is in close agreement with findings of Garraway et al., who also recently identified overexpression of TFF3 at the protein level in prostate cancer [31]. These similar findings occurred in both studies despite the facts that two different patient populations were studied and two different antibodies were used. We also present the first use of our tissue microarray software analysis package, TMAJ, which allows scoring of TMA Images over the internet. Finally, we also demonstrated the feasibility of using the ACIS by Chromavision Medical Systems to automate the scoring of TMA spots using brightfield microscopy.

The percentage of cells staining positive and percentage of cells staining strong correlated inversely with pathological stage and preoperative serum PSA when Group I and Group II patients were analyzed together. However, when separated by time of surgery the inverse relation was present only in the Group II (those with long term follow-up). Since the staining levels did not correlate with outcome, the inverse relation between TFF3 staining levels and pathological stage does not appear to be clinically important. The fact that Garraway et al. also did not find TFF3 to be a prognostic marker in their study [31] indicates that this lack of prognostic value may not simply be a feature of our study population.

While this study does not indicate whether TFF3 is facilitating carcinogenesis or simply represents a passive marker linked to some other relevant pathway, it does identify a subset of prostate cancers that overexpress the protein as compared to normal epithelium. Atypical expression of all three known trefoil factor peptides has been associated with a range of inflammatory diseases and adenocarcinomas [12,13,17,24–30].

TABLE II. Summary of Immunostaining by Tissue Type

Type	n	Mean percent positive	Mean percent strong	Number of cases staining negative	Number of cases with >20% positive cells	Number of cases with >20% strong positive cells
Normal	272	11.2 ± 17.0	3.1 ± 8.3	75 (27.6%)	51 (18.8%)	13 (4.8%)
Tumor	268	35.8 ± 37.7	21.0 ± 32.3	65 (24.3%)	126 (47.0%)	84 (31.3%)
Atrophy	76	7.1 ± 17.4	1.8 ± 9.9	50 (65.8%)	5 (6.6%)	2 (2.6%)
PIN	32	35.2 ± 37.2	13.9 ± 20.9	6 (18.8%)	15 (46.9%)	8 (25.0%)
Met: all	61	35.9 ± 39.0	19.3 ± 30.7	16 (26.2%)	28 (45.9%)	17 (27.9%)
Met: regional	51	29.9 ± 35.0	13.7 ± 26.1	14 (27.5%)	21 (41.2%)	10 (19.6%)
Met: distant	10	66.3 ± 46.0	47.6 ± 38	2 (20.0%)	7 (70.0%)	7 (70.0%)

Met, metastatic lesions; regional, pelvic lymph nodes; distant, bone or distant soft tissue metastasis. Mean percent positive indicates mean percentage of cells staining positive for the given tissue type across all specimens.

TABLE III. Correlations Between Trefoil Factor 3 (TFF3) Staining and Clinical and Pathological Variables

	Tumor		Normal	
	% Positive	% Strong	% Positive	% Strong
Preoperative serum PSA*	0.0084	0.0354	0.4032	0.2806
Gleason grade*	0.9468	0.7589	0.0552	0.0748
Surgical margin involvement	0.5370	0.1773	0.0342	0.0785
Overall path stage*,[a]	0.0054	0.0018	0.0298	0.1329
Capsular penetration	0.0013	0.0007	0.0303	0.0631
Seminal vesicle involvement	0.0037	0.0024	0.1507	0.2301
Presence of LN metastasis	0.0037	0.0014	0.8471	0.5281
Development of distant metastasis	0.8717	0.8678	0.9702	0.6829
Death due to prostate cancer	0.7812	0.9106	0.8256	0.8549

*Kruskal–Wallis test for more than two categories, otherwise, Wilcoxon Rank Sum. Table shows *P* values.
[a]American Joint Committee on Cancer (AJCC) 2002 Staging.

However, no discrete function has been ascribed to this altered expression in cancer. TFF3 function in normal cells ranges from mucosal protection and maintenance to neurotransmission [14]. One or more of these functions may explain the low-level expression in the normal prostate. Other reported characteristics of TFF3 may prove more directly relevant to carcinogenesis. For example, TFF3 can trigger phosphorylation of the epidermal growth factor receptor, providing protection against p53 independent apoptosis [51]. Also, TFF3 has been reported to induce sustained tyrosine phosphorylation of β and γ catenins [52], which would result in the down regulation of various cell adhesion molecules. This phosphorylation may be responsible for the enhanced dispersion necessary to promote greater motility, which is thought to be a key property of cancer cell invasiveness and metastatic potential [53].

Tissue microarrays are proving instrumental in the ability to increase the throughput of analysis of human clinical specimens as related to disease biology and clinical outcome [54–59]. Yet, TMA technology presents problems in data analysis and management. To more fully exploit the potential information derived from TMA analysis, several groups have been working on developing software tools to facilitate scoring of digitally imaged TMA spots with simultaneous storage of data directly into a relational database or spreadsheet [48,49,60,61]. We have been developing our own version of this approach in which the software programs and database are referred to as TMAJ [36,37] (J standing for the Java programming language and Johns Hopkins) and present here the first study using these tools. TMAJ is designed as a comprehensive, secure, HIPPA-compliant, tissue microarray database that can store clinical and pathological data from multiple organ systems and that facilitates viewing and scoring of TMA Images over the internet. The database is compatible with emerging standards for TMA data structures [62]. It also provides a tool for export of scoring data linked to relevant clinical-pathological information, in a tab-delimited or spreadsheet form, amendable to statistical analysis and data-sharing. In

TABLE IV. Relation of TFF3 Staining to Time to Biochemical Recurrence After Radical Prostatectomy

	Time to biochemical recurrence (years)							
	Any positive TFF3 staining				Strong positive TFF3 staining			
	N	Median	Mean	SD	N	Median	Mean	SD
Staining negative	49	3	4.4	3.3	82	3	4.4	3.4
Staining positive (≤20% tumor cells)	46	4	4.2	3.2	33	3	3.8	2.5
Staining positive (>20% tumor cells)	56	3	4	2.8	36	3	3.9	2.8
Total	151				151			

No significant difference (Kruskal–Wallis) among groups ($P = 0.96$ for any positive staining group, and $P = 0.91$ for strong positive staining group). There are 151 of the 161 patients in Group II that had data from tumor tissues available for analysis.

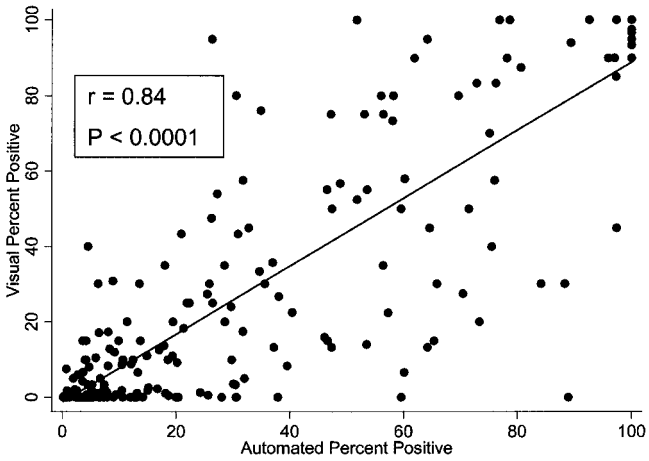

Fig. 5. Scatter plot of average visual estimation of percent positive and automated assessment using cytokeratin normalization. The individual data points represent the mean of TMA spots from each patient sample. Automated Percent Positive scores that were above 100 (indicating greater TFF3 area than Keratin 8 area) were converted to a score of 100.

brief, this software and database facilitate rapid assessment of biomarkers using TMAs.

While TMAJ and other databases facilitate data handling and online image scoring by a pathologist or trained technician, it is clear that in order for biomarkers to be more rapidly screened in large numbers of clinical specimens, more automated systems of immunohistochemical scoring are needed. Recently Camp et al. presented a powerful approach to automated TMA Image analysis and quantification using TMAs stained by immunofluroescence [63]. While this method is extremely promising, there have been no studies using automated or semi-automated scoring of TMAs prepared for conventional brightfield microscopy. In this study, we show the first example of this semi-automated TMA immunohistochemistry scoring using the ACIS I from Chromavision.

ACKNOWLEDGMENTS

The authors thank Brian Razzaque, Joe Zimmerman, and Chris White from Vision Multimedia Technologies LLC for help with all aspects of tissue microarray database and software design. We acknowledge the Johns Hopkins Tissue Microarray core facility and thank Marcella Southerland Gerrun March, and Christina Bennett for diligent help with tissue and tissue microarray design and construction. We thank Elizabeth Barnes for help in obtaining clinical follow-up data.

TMA images and scoring data are available for online browsing and download at ''http://tmaj.pathology.jhmi.edu'' by clicking on the Images application, logging on as guest, (user name & password) and clicking on the published Images button.

REFERENCES

1. Chinery R, Bates PA, De A, Freemont PS. Characterisation of the single copy trefoil peptides intestinal trefoil factor and pS2 and their ability to form covalent dimers. FEBS Lett 1995;357(1):50–54.
2. Graness A, Chwieralski CE, Reinhold D, Thim L, Hoffmann W. Protein kinase C and ERK activation are required for TFF-peptide-stimulated bronchial epithelial cell migration and tumor necrosis factor-alpha-induced interleukin-6 (IL-6) and IL-8 secretion. J Biol Chem 2002;277(21):18440–18446.
3. Hauser F, Poulsom R, Chinery R, Rogers LA, Hanby AM, Wright NA, Hoffmann W. hP1.B, a human P-domain peptide homologous with rat intestinal trefoil factor, is expressed also in the ulcer-associated cell lineage and the uterus. Proc Natl Acad Sci USA 1993;90(15):6961–6965.
4. Hoffmann W, Jagla W. Cell type specific expression of secretory TFF peptides: Colocalization with mucins and synthesis in the brain. Int Rev Cytol 2002;213:147–181.
5. Hoffmann W, Jagla W, Wiede A. Molecular medicine of TFF-peptides: From gut to brain. Histol Histopathol 2001;16(1):319–334.
6. Suemori S, Lynch-Devaney K, Podolsky DK. Identification and characterization of rat intestinal trefoil factor: Tissue- and cell-specific member of the trefoil protein family. Proc Natl Acad Sci USA 1991;88(24):11017–11021.
7. Podolsky DK, Lynch-Devaney K, Stow JL, Oates P, Murgue B, DeBeaumont M, Sands BE, Mahida YR. Identification of human intestinal trefoil factor. Goblet cell-specific expression of a peptide targeted for apical secretion. J Biol Chem 1993;268(9):6694–6702.
8. Xian CJ, Howarth GS, Mardell CE, Cool JC, Familari M, Read LC, Giraud AS. Temporal changes in TFF3 expression and jejunal morphology during methotrexate-induced damage and repair. Am J Physiol 1999;277(4 Pt 1):G785–G795.
9. Babyatsky MW, deBeaumont M, Thim L, Podolsky DK. Oral trefoil peptides protect against ethanol- and indomethacin-induced gastric injury in rats. Gastroenterology 1996;110(2):489–497.
10. Dignass A, Lynch-Devaney K, Kindon H, Thim L, Podolsky DK. Trefoil peptides promote epithelial migration through a transforming growth factor beta-independent pathway. J Clin Invest 1994;94(1):376–383.
11. Nusrat A, Delp C, Madara JL. Intestinal epithelial restitution. Characterization of a cell culture model and mapping of cytoskeletal elements in migrating cells. J Clin Invest 1992;89(5):1501–1511.
12. Wright NA, Poulsom R, Stamp G, Van Noorden S, Sarraf C, Elia G, Ahnen D, Jeffery R, Longcroft J, Pike C, et al. Trefoil peptide gene expression in gastrointestinal epithelial cells in inflammatory bowel disease. Gastroenterology 1993;104(1):12–20.
13. Rio MC, Chenard MP, Wolf C, Marcellin L, Tomasetto C, Lathe R, Bellocq JP, Chambon P. Induction of *pS2* and *hSP* genes as markers of mucosal ulceration of the digestive tract. Gastroenterology 1991;100(2):375–379.
14. Schwarzberg H, Kalbacher H, Hoffmann W. Differential behavioral effects of TFF peptides: Injections of synthetic TFF3 into the rat amygdala. Pharmacol Biochem Behav 1999;62(1):173–178.
15. Jagla W, Wiede A, Dietzmann K, Rutkowski K, Hoffmann W. Co-localization of TFF3 peptide and oxytocin in the human hypothalamus. FASEB J 2000;14(9):1126–1131.
16. Wiede A, Hinz M, Canzler E, Franke K, Quednow C, Hoffmann W. Synthesis and localization of the mucin-associated

TFF-peptides in the human uterus. Cell Tissue Res 2001;303(1): 109–115.

17. Poulsom R, Hanby AM, Lalani EN, Hauser F, Hoffmann W, Stamp GW. Intestinal trefoil factor (TFF 3) and pS2 (TFF 1), but not spasmolytic polypeptide (TFF 2) mRNAs are co-expressed in normal, hyperplastic, and neoplastic human breast epithelium. J Pathol 1997;183(1):30–38.
18. Schwarz H, Jagla W, Wiede A, Hoffmann W. Ultrastructural co-localization of TFF3-peptide and oxytocin in the neural lobe of the porcine pituitary. Cell Tissue Res 2001;305(3):411–416.
19. Devine DA, High AS, Owen PJ, Poulsom R, Bonass WA. Trefoil factor expression in normal and diseased human salivary glands. Hum Pathol 2000;31(4):509–515.
20. Jagla W, Wiede A, Hinz M, Dietzmann K, Gulicher D, Gerlach KL, Hoffmann W. Secretion of TFF-peptides by human salivary glands. Cell Tissue Res 1999;298(1):161–166.
21. Langer G, Walter S, Behrens-Baumann W, Hoffmann W. TFF peptides. New mucus-associated secretory products of the conjunctiva. Ophthalmologe 2001;98(10):976–979.
22. Jagla W, Wiede A, Hoffmann W. Localization of TFF3 peptide to porcine conjunctival goblet cells. Cell Tissue Res 1999;296(3): 525–530.
23. dos Santos Silva E, Ulrich M, Doring G, Botzenhart K, Gott P. Trefoil factor family domain peptides in the human respiratory tract. J Pathol 2000;190(2):133–142.
24. May FE, Westley BR. Expression of human intestinal trefoil factor in malignant cells and its regulation by oestrogen in breast cancer cells. J Pathol 1997;182(4):404–413.
25. Taupin D, Pedersen J, Familari M, Cook G, Yeomans N, Giraud AS. Augmented intestinal trefoil factor (TFF3) and loss of pS2 (TFF1) expression precedes metaplastic differentiation of gastric epithelium. Lab Invest 2001;81(3):397–408.
26. Terris B, Blaveri E, Crnogorac-Jurcevic T, Jones M, Missiaglia E, Ruszniewski P, Sauvanet A, Lemoine NR. Characterization of gene expression profiles in intraductal papillary-mucinous tumors of the pancreas. Am J Pathol 2002;160(5):1745–1754.
27. Taupin D, Ooi K, Yeomans N, Giraud A. Conserved expression of intestinal trefoil factor in the human colonic adenoma-carcinoma sequence. Lab Invest 1996;75(1):25–32.
28. Yamachika T, Werther JL, Bodian C, Babyatsky M, Tatematsu M, Yamamura Y, Chen A, Itzkowitz S. Intestinal trefoil factor: A marker of poor prognosis in gastric carcinoma. Clin Cancer Res 2002;8(5):1092–1099.
29. Colombel M, Dante R, Bouvier R, Ribieras S, Pangaud C, Marechal JM, Lasne Y. Differential RNA expression of the *pS2* gene in the human benign and malignant prostatic tissue. J Urol 1999;162(3 Pt 1):927–930.
30. Bonkhoff H, Stein U, Welter C, Remberger K. Differential expression of the pS2 protein in the human prostate and prostate cancer: Association with premalignant changes and neuroendocrine differentiation. Hum Pathol 1995;26(8):824–828.
31. Garraway IP, Seligson D, Said J, Horvath S, Reiter RE. Trefoil factor 3 is overexpressed in human prostate cancer. The Prostate 2004; this issue.
32. Luo J, Duggan DJ, Chen Y, Sauvageot J, Ewing CM, Bittner ML, Trent JM, Isaacs WB. Human prostate cancer and benign prostatic hyperplasia: Molecular dissection by gene expression profiling. Cancer Res 2001;61(12):4683–4688.
33. Dhanasekaran SM, Barrette TR, Ghosh D, Shah R, Varambally S, Kurachi K, Pienta KJ, Rubin MA, Chinnaiyan AM. Delineation of prognostic biomarkers in prostate cancer. Nature 2001; 412(6849):822–826.
34. Welsh JB, Sapinoso LM, Su AI, Kern SG, Wang-Rodriguez J, Moskaluk CA, Frierson HF, Jr., Hampton GM. Analysis of gene expression identifies candidate markers and pharmacological targets in prostate cancer. Cancer Res 2001;61(16):5974–5978.
35. Rhodes DR, Barrette TR, Rubin MA, Ghosh D, Chinnaiyan AM. Meta-analysis of microarrays: Interstudy validation of gene expression profiles reveals pathway dysregulation in prostate cancer. Cancer Res 2002;62(15):4427–4433.
36. Morgan JD, Iacobuzio-Donahue C, Razzaque B, Faith D, De Marzo AM. TMAJ: Open source software to manage a tissue microarray database. October 8–10, 2003; Pittsburgh, PA.
37. De Marzo AM, Morgan JD, Razzaque B, White C, Zimmerman J, Bennett CJ, Fedor H, Faith D. TMAJ: A set of open source software tools to manage a multiple-organ, scalable, secure, mulitple-user tissue microarray database. October 2–4, 2002; Pittsburgh, PA.
38. Bauer KD, de la Torre-Bueno J, Diel IJ, Hawes D, Decker WJ, Priddy C, Bossy B, Ludmann S, Yamamoto K, Masih AS, Espinoza FP, Harrington DS. Reliable and sensitive analysis of occult bone marrow metastases using automated cellular imaging. Clin Cancer Res 2000;6(9):3552–3559.
39. Sun W, Zhang PL, Herrera GA. p53 protein and Ki-67 overexpression in urothelial dysplasia of bladder. Appl Immunohistochem Mol Morphol 2002;10(4):327–331.
40. Hilbe W, Gachter A, Duba HC, Dirnhofer S, Eisterer W, Schmid T, Mildner A, Bodner J, Woll E. Comparison of automated cellular imaging system and manual microscopy for immunohistochemically stained cryostat sections of lung cancer specimens applying p53, ki-67, and p120. Oncol Rep 2003; 10(1): 15–20.
41. Wang S, Saboorian MH, Frenkel EP, Haley BB, Siddiqui MT, Gokaslan S, Wians FH, Jr., Hynan L, Ashfaq R. Assessment of HER-2/neu status in breast cancer. Automated Cellular Imaging System (ACIS)-assisted quantitation of immunohistochemical assay achieves high accuracy in comparison with fluorescence in situ hybridization assay as the standard. Am J Clin Pathol 2001;116(4):495–503.
42. Pound CR, Partin AW, Eisenberger MA, Chan DW, Pearson JD, Walsh PC. Natural history of progression after PSA elevation following radical prostatectomy. JAMA 1999;281(17):1591–1597.
43. Kononen J, Bubendorf L, Kallioniemi A, Barlund M, Schraml P, Leighton S, Torhorst J, Mihatsch MJ, Sauter G, Kallioniemi OP. Tissue microarrays for high-throughput molecular profiling of tumor specimens. Nat Med 1998;4(7):844–847.
44. Zha S, Gage WR, Sauvageot J, Saria EA, Putzi MJ, Ewing CM, Faith DA, Nelson WG, De Marzo AM, Isaacs WB. Cyclooxygenase-2 is up-regulated in proliferative inflammatory atrophy of the prostate, but not in prostate carcinoma. Cancer Res 2001; 61(24):8617–8623.
45. De Marzo AM, Fedor HH, Gage WR, Rubin MA. Inadequate formalin fixation decreases reliability of p27 immunohistochemical staining: Probing optimal fixation time using high-density tissue microarrays. Hum Pathol 2002;33(7):756–760.
46. Ruijter ET, Miller GJ, Aalders TW, van de Kaa CA, Schalken JA, Debruyne FM, Boon ME. Rapid microwave-stimulated fixation of entire prostatectomy specimens. Biomed-II MPC Study Group. J Pathol 1997;183(3):369–375.
47. Bova GS, Fox WM, Epstein JI. Methods of radical prostatectomy specimen processing: A novel technique for harvesting fresh prostate cancer tissue and review of processing techniques. Mod Pathol 1993;6(2):201–207.

48. Manley S, Mucci NR, De Marzo AM, Rubin MA. Relational database structure to manage high-density tissue microarray data and images for pathology studies focusing on clinical outcome: The Prostate Specialized Program of Research Excellence model. Am J Pathol 2001;159(3):837–843.
49. Bova GS, Parmigiani G, Epstein JI, Wheeler T, Mucci NR, Rubin MA. Web-based tissue microarray image data analysis: Initial validation testing through prostate cancer Gleason grading. Hum Pathol 2001;32(4):417–427.
50. Luo J, Zha S, Gage WR, Dunn TA, Hicks JL, Bennett CJ, Ewing CM, Platz EA, Ferdinandusse S, Wanders RJ, Trent JM, Isaacs WB, De Marzo AM. Alpha-methylacyl-CoA racemase: A new molecular marker for prostate cancer. Cancer Res 2002; 62(8):2220–2226.
51. Taupin DR, Kinoshita K, Podolsky DK. Intestinal trefoil factor confers colonic epithelial resistance to apoptosis. Proc Natl Acad Sci USA 2000;97(2):799–804.
52. Liu D, el-Hariry I, Karayiannakis AJ, Wilding J, Chinery R, Kmiot W, McCrea PD, Gullick WJ, Pignatelli M. Phosphorylation of beta-catenin and epidermal growth factor receptor by intestinal trefoil factor. Lab Invest 1997;77(6):557–563.
53. Partin AW, Schoeniger JS, Mohler JL, Coffey DS. Fourier analysis of cell motility: Correlation of motility with metastatic potential. Proc Natl Acad Sci USA 1989;86(4):1254–1258.
54. Kononen J, Bubendorf L, Kallioniemi A, Barlund M, Schraml P, Leighton S, Torhorst J, Mihatsch MJ, Sauter G, Kallioniemi OP. Tissue microarrays for high-throughput molecular profiling of tumor specimens. Nat Med 1998;4(7):844–847.
55. Kallioniemi OP. Biochip technologies in cancer research. Ann Med 2001;33(2):142–147.
56. Rimm DL, Camp RL, Charette LA, Olsen DA, Provost E. Amplification of tissue by construction of tissue microarrays. Exp Mol Pathol 2001;70(3):255–264.
57. Rimm DL, Camp RL, Charette LA, Costa J, Olsen DA, Reiss M. Tissue microarray: A new technology for amplification of tissue resources. Cancer J 2001;7(1):24–31.
58. Torhorst J, Bucher C, Kononen J, Haas P, Zuber M, Kochli OR, Mross F, Dieterich H, Moch H, Mihatsch M, Kallioniemi OP, Sauter G. Tissue microarrays for rapid linking of molecular changes to clinical endpoints. Am J Pathol 2001;159(6):2249–2256.
59. Skacel M, Skilton B, Pettay JD, Tubbs RR. Tissue microarrays: A powerful tool for high-throughput analysis of clinical specimens: A review of the method with validation data. Appl Immunohistochem Mol Morphol 2002;10(1):1–6.
60. Liu CL, Prapong W, Natkunam Y, Alizadeh A, Montgomery K, Gilks CB, van de Rijn M. Software tools for high-throughput analysis and archiving of immunohistochemistry staining data obtained with tissue microarrays. Am J Pathol 2002;161(5):1557–1565.
61. Rhodes DR, Sanda MG, Otte AP, Chinnaiyan AM, Rubin MA. Multiplex biomarker approach for determining risk of prostate-specific antigen-defined recurrence of prostate cancer. J Natl Cancer Inst 2003;95(9):661–668.
62. Berman JJ, Edgerton ME, Friedman BA. The tissue microarray data exchange specification: A community-based, open source tool for sharing tissue microarray data. BMC Med Inform Decis Making 2003;3(1):5.
63. Camp RL, Chung GG, Rimm DL. Automated subcellular localization and quantification of protein expression in tissue microarrays. Nat Med 2002;8(11):1323–1327.